

Mg(OH)₂ Nanorods Synthesized by A Facile Hydrothermal Method in the Presence of CTAB

Hassouna Dhaouadi^{1,*}, Hedia Chaabane², Fathi Touati¹

(Received 28 June 2011; accepted 23 August 2011; published online 4 September 2011.)

Abstract: Magnesium hydroxide (Mg(OH)₂) nanorods were synthesized by a simple and facile hydrothermal method in the presence of cetyltrimethylammonium bromide (CTAB) as a surfactant. Nanorods of magnesium oxide MgO were also induced by thermal decomposition of Mg(OH)₂ nanorods at 700°C. By using disk diffusion technique, the Mg(OH)₂ nanorods were found to exhibit higher antibacterial efficiency against several tested bacterial strains.

Keywords: Nanorods; Morphology; Hydrothermal synthesis

Citation: Hassouna Dhaouadi, Hedia Chaabane and Fathi Touati, "Mg(OH)₂ Nanorods Synthesized by A Facile Hydrothermal Method in the Presence of CTAB", *Nano-Micro Lett.* 3 (3), 153-159 (2011). <http://dx.doi.org/10.3786/nml.v3i3.p153-159>

Introduction

The special attributes of nanomaterials arise due to their unique physical properties like electrical conductivity, optical band gap, magnetic properties and superior mechanical properties. Among various nanomaterials, magnesium hydroxide nanostructure has received a special interest for their attractive scientific and technological aspects in different fields. Magnesium hydroxide is used as halogen-free flame retardants for polymers, electric cables, building and decoration materials [1], preparing foodstuff starch esters [2] and treating wastewater [3]. The size and the morphology of the grain play a crucial role in all these applications. Currently, the synthesis of Mg(OH)₂ nanomaterials is being carried out by different techniques to achieve desired size and shape. Different methods, such as solvothermal method [4], reverse precipitation [5], hydrothermal route [6] and solution based chemical process [7] were adopted by scientists to prepare Mg(OH)₂ nanomaterials. The preparation of one dimensional (1D) nanostructures, such as nanowires, nanorods and nanotubes triggered in-

tensive attentions owing to their potential applications in various fields, such as nanodevice, nanocable, and nanobiosensor [8,9].

With the emergence and the increase of microbial organisms, many researchers have been focusing on the new and effective antimicrobial reagent developments. Inorganic antibacterial agents received more and more recognition as antibacterial products [10,11]. Inorganic nanoparticles, whose structures exhibit novel physical, chemical and biological properties, have attracted much interest. Among the inorganic antibacterial agents, Mg(OH)₂ is well known as an effective antibacterial agent [12].

In this paper, we describe a simple method to synthesize Mg(OH)₂ nanorods using the hydrothermal method in the presence of CTAB as surfactant. The properties of product were investigated and the formation mechanism was discussed on the basis of our experimental results. The antibacterial activities of the Mg(OH)₂ nanorods were investigated using a disc diffusion method.

¹“Laboratoire des Matériaux Utiles” Institut National de Recherche et d’Analyse Physico-chimique, Pôle technologique de Sidi-Thabet, 2020, Tunis, Tunisie

²“Laboratoire de Microbiologie” Institut National de Recherche et d’Analyse Physico-chimique, Pôle technologique de Sidi-Thabet, 2020, Tunis, Tunisie

*Corresponding author. E-mail: dhaouadihassouna@yahoo.fr

Experimental procedure

Hydrothermal synthesis

The synthesis of nanorods $\text{Mg}(\text{OH})_2$ was performed by the hydrothermal method. However, 1.37 mmol of commercial MgO powder was dispersed in aqueous solution of CTAB (1.37 mmol/20 ml). After sufficient stirring, the solution was transferred into a Teflon-lined stainless steel autoclave. The autoclave was sealed and introduced in oven maintained at 200°C for 24 h, and then left to cool to room temperature. The resulted powders were filtered, washed with distilled water to remove the ions possibly remaining in the final powder, and finally dried in vacuum at 80°C for 2 h. The chemical equation of reaction process for fabricating magnesium hydroxide nanorods can be described as follows: $\text{MgO} + \text{H}_2\text{O} = \text{Mg}(\text{OH})_2$

Characterization

X-ray powder diffraction (XRD) pattern was determined using a Panalytical XPERT PRO MPD diffractometer operating with Cu K_α radiation ($\lambda=0.15406\text{ nm}$). Infrared spectra (IR) of the studied samples were recorded in the wave number range $4000\sim 400\text{ cm}^{-1}$ with a “Nicolet 380 Spectrometer” using samples dispersed in pure KBr pellets. Thermal analysis was performed using the “Setaram setsys 1750” operating from room temperature to 800°C at an average heating rate of 10°C/min. The morphology of the sample was carried out using a FEI Quanta 200 environmental scanning electron microscope (SEM). Transmission electron microscopy (TEM) studies were recorded on JEOL 100 CX II electron microscope operated at 200 KV. One droplet of the powder dispersed in $\text{CH}_3\text{CH}_2\text{OH}$ was deposited onto a carbon-coated copper grid and left to dry in air.

The disc diffusion method was used to evaluate the antimicrobial activity of the $\text{Mg}(\text{OH})_2$ nanorods against different strains of bacteria: *Staphylococcus aureus* ATCC 6538, *Enterococcus faecalis* ATCC 29212, *Enterococcus faecium* ATCC 19434, *Bacillus cereus*, *Bacillus subtilis*, *Staphylococcus fecalis*, *Streptococcus B* (*Streptococcus agalactiae*). Suspensions of $\text{Mg}(\text{OH})_2$ nanomaterials were prepared in the LB culture broth and well dispersed using ultrasonification for 20 min and autoclaved. All the microorganisms were cultured overnight at 37°C in the nutritive medium and used as inoculums; the turbidity of the suspensions was adjusted to the McFerland 0.5 turbidity standard. These suspensions with an approximately concentration of 10^8 colony forming units per milliliter (CFU ml^{-1}) were used to inoculate Mueller-Hinton Agar. Two discs impregnated one with the ampicillin used as positive control and the other with the $\text{Mg}(\text{OH})_2$ suspension were placed on the

surface of these plates and incubated at 37°C for 18 h. The diameter of the zone of growth inhibition around the discs was measured.

Results and discussion

X ray diffraction

Figure 1 shows XRD patterns of the as prepared $\text{Mg}(\text{OH})_2$ nanorods and the same samples after calcinations at different temperatures. As seen in Fig. 1(a) all diffraction peaks can be perfectly indexed in a hexagonal structure space group P-3m1(164) (JCPDS file No. 00-044-1482) with unit cell parameters (a)=3.1442 Å and (c)=4.7770 Å. No characteristic peaks of other phases are detected, which indicates a high purity of the obtained $\text{Mg}(\text{OH})_2$ materials. Significant XRD peaks at $2\theta=37.972$, 18.574, 50.903, 58.593°, could be assigned to the Bragg peaks (101), (001), (102), and (110), respectively. These peaks were rather broad, indicating the nanocrystallite size of the as synthesized compound. The average crystallite size was estimated to be 40 nm according to the (101) reflection using the Debye Scherrer approximation [13]. This value can be attributed to the nanorod diameter, as confirmed by TEM studies. It is noted that the relative intensities of some peaks differ from the standard pattern of the bulk material, which should be caused by preferred orientation and distribution of the $\text{Mg}(\text{OH})_2$ nanocrystals.

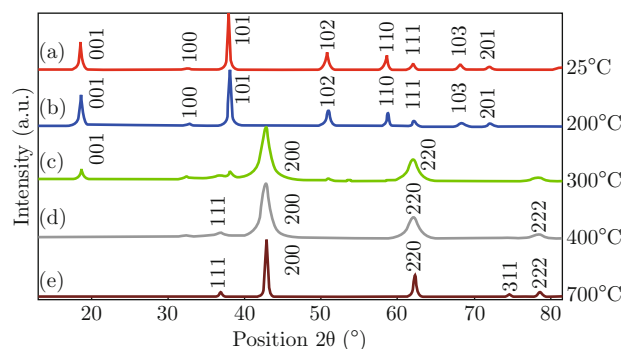


Fig. 1 X-ray diffraction patterns of the as prepared $\text{Mg}(\text{OH})_2$ nanorods (a) and the same samples calcined at different temperatures (b) 200°C; (c) 300°C; (d) 400°C; (e) 700°C.

The slow calcination of $\text{Mg}(\text{OH})_2$ from room temperature to 700°C (Fig. 1(e)) provides the pure magnesium oxide MgO with relatively uniform morphology. Indeed, when the $\text{Mg}(\text{OH})_2$ is heated in air, the following reaction takes place: $\text{Mg}(\text{OH})_2 = \text{MgO} + \text{H}_2\text{O}$. The X-ray diffraction pattern of the MgO nanorods is illustrated in Fig. 1(e). All peaks can be well indexed to the cubic structure, with space group Fm-3m (225). The unit cell parameters are: (a)=(b)=(c)=4.2123 Å and

the volume $V=74.74 \text{ \AA}^3$ of MgO (JCPDS file No. 01-078-0430). Six slightly broad diffraction peaks corresponding to 2θ angles: 36.97, 42.98, 62.32, 74.74 and 78.71° can be readily indexed to (111), (200), (220), (311) and (222) respectively. No characteristic peaks from any other phases of MgO and impurities have been observed, indicating the high purity of the obtained cubic MgO nanorods. The average crystallite size is estimated to 35 nm according to the (200) reflection using the Debye Scherrer's formula [13]. In addition, it is noted that the intensity of (200) and (220) peaks is 29.54% less strong than the standard value of PDF card (45.1%), suggesting that the MgO product might have a preferential orientation.

IR absorption spectroscopy

Figure 2 displays the IR spectra of the as prepared Mg(OH)₂ nanorods and the same samples after calcinations at different temperatures. Figure 2(a) shows the vibration band characteristics of organic cation (CTA⁺), O-H groups and the octahedron MgO₆ entities. The stretching vibrations of the Mg-O bands are observed at 820 and 680 cm⁻¹ while their bending modes are located at 420 cm⁻¹. The free hydroxyl group (-OH) stretching mode appears as a sharp peak at 3700 cm⁻¹ [14,15]. When the temperature increases, the peak intensity of the free hydroxyl group stretching

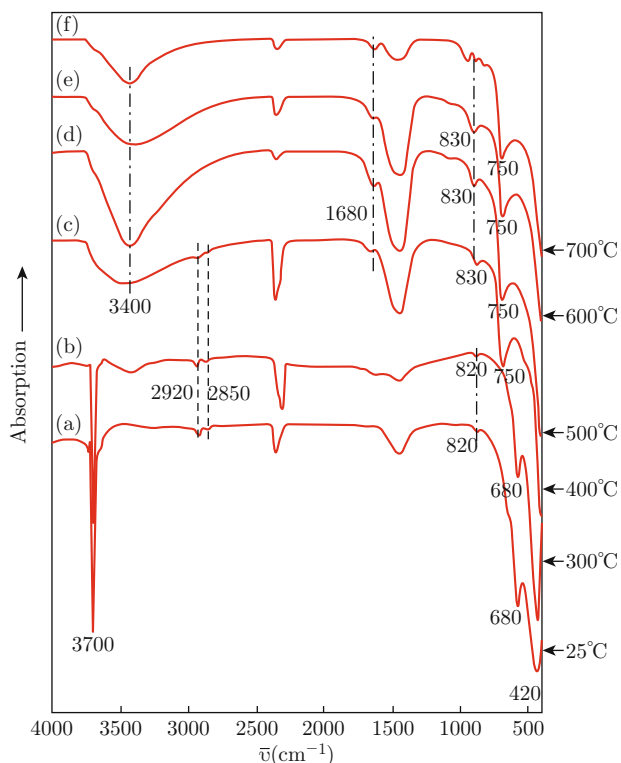


Fig. 2 IR spectra of the as prepared Mg(OH)₂ nanorods: (a) and the same samples calcined at different temperatures; (b) 300°C; (c) 400°C; (d) 500°C; (e) 600°C; (e) 700°C.

mode becomes smaller and finally disappears when the temperature reaches 400°C. As the temperature increases, the stretching as well as the bending modes of Mg-O entities shift to higher frequencies (830 and 750 cm⁻¹) (Fig. 2(c)-(f)). This can be explained by the disparition of the H-bonds of O-H...O type, which maintain the inorganic parallel layers as shown in Fig. 5. The broad bands observed at high frequencies in the IR spectrum extending from 3400 to 3200 cm⁻¹, are due to the symmetric and asymmetric stretching modes of the hydroxyl group, which reveal the existence of adsorbed water molecules on the MgO surface as seen in Fig. 2(d), 2(e), 2(f). The bending modes of the adsorbed water molecules appear as a weak band around 1680 cm⁻¹.

The two weak bands observed in the IR spectra (Fig. 2(a)-(c)) at high frequencies (2920 and 2850 cm⁻¹), can be attributed to the stretching mode of (-CH₂) and (CH₃) groups of residual organic surfactant, while their bending modes ($\delta(-CH_2)$, $\delta(CH_3)$) appear in the range 1700~1400 cm⁻¹ [16]. Stretching and bending modes of the organic surfactant disappear progressively when the temperature increases.

Morphology

In order to investigate the morphology of Mg(OH)₂ product, SEM characterizations were performed (Fig. 3(a)). The sample mainly consists of nanorod aggregates, with different sizes. Additional informations concerning the microstructure are obtained from TEM images (Fig. 3(b)). The obtained product has a nanorod shape with a diameter between 10 and 40 nm and a length of up to 300 nm (Fig. 3(b) inset).

Figure 3(c) represents the SEM image of calcinated Mg(OH)₂ materials. The obtained MgO nanomaterials present a nanorod shape, which indicates that the nanomaterials preserve the same morphology of Mg(OH)₂ nanorods during the calcination process at about 700°C. This behaviour can be explained by the low heating rate (5°C/min), the cooling rate (5°C/min) and the long calcination time (4 h). While in the case of Mg(OH)₂ nanorods prepared by liquid-solid solution arc discharge technique, the rod shape of Mg(OH)₂ could not be preserved during the heating process up to 650°C [17]. Many studies have demonstrated the original morphology of Mg(OH)₂ precursor and the controlled conditions of the dehydration process playing a key role in the crystal morphology and the related properties of the final MgO products [18].

Thermal analysis

In order to examine the thermal stability of the compound Mg(OH)₂, DTA/TG were carried out between 25°C and 800°C (Fig. 4). Mg(OH)₂ sample is still stable up to 155°C. Then, the endothermic peak corresponding

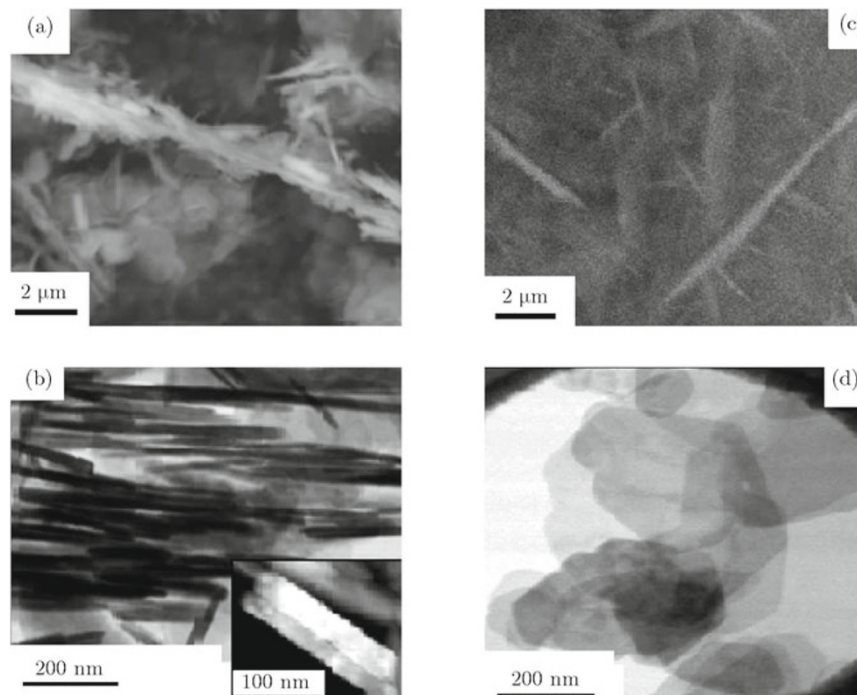


Fig. 3 (a) SEM image of Mg(OH)₂ nanorods; (b) TEM micrograph of Mg(OH)₂ nanorods; (c) SEM image of MgO nanorods; (d) TEM picture of Mg(OH)₂ nanoplatelets.

to the removal of the adsorbed water molecules takes place between 150~280°C. This phenomenon is well observed in the TG curve as a slight weight loss between 150~280°C. The major weight loss step is found in the temperature range of 280~450°C, which is due to the transition phase.

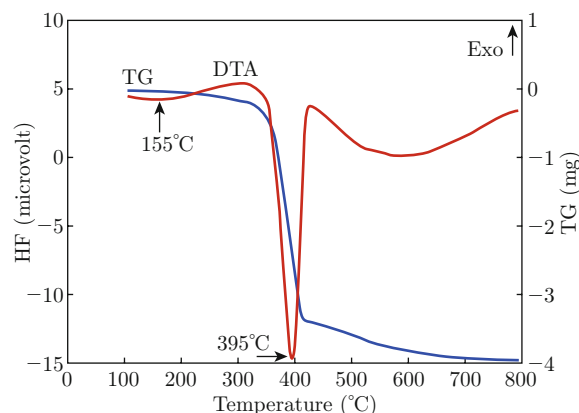
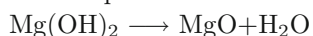


Fig. 4 DTA/TGA thermograms of Mg(OH)₂ nanorods.

The TG curve exhibits a total mass loss equal to 33.03 %, which is greater than that calculated mass loss (31.03%) attributed to the complete dehydroxylation process of Mg(OH)₂. The excess of mass loss (2.00%) could be attributed to the residual organic entities adsorbed on the nanorod surfaces. The removal of water in a large domain of temperature is also observed

in other compounds such as WO₃.H₂O nanomaterials [19]. This can be explained by the slow dehydroxylation process. However, the hydrogen bonds of O-H...O type which connect two adjacent layers (Fig. 5) were partially broken and released progressively water molecules. The broad endothermic peak around 600°C probably corresponds to the release of remained -OH groups from brucite phase, to provide the new phase MgO.

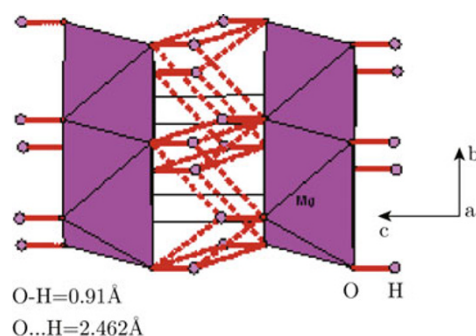


Fig. 5 Schematic representation of hexagonal Mg(OH)₂ unit cell along the a axis.

In order to put forward an interpretation of thermal phenomenon observed on the two curves (DTA/TGA), X-ray diffraction analysis has been performed at different temperatures. Several samples of partial decomposed Mg(OH)₂ were heated in electric oven (under air atmosphere) at different temperatures: 25, 200, 300, 400, 700°C, and then they were immediately submitted

to XRD study as shown in Fig. 1. The X-ray diffraction of the product calcined at 200°C is very similar to that of the starting sample (25°C), this means that the brucite is stable until 200°C, and no structural transformation undergoes. After calcination at 300°C the intensities of the reflections due to the brucite phase $\text{Mg}(\text{OH})_2$ corresponding to (001), (100), (101), (102) and (110) was significantly attenuated. The rest of the peaks disappears ((201), (103) and (111)). This behaviour could be explained by the fact that the dehydroxylation process is not achieved at this stage. As the temperature increases, the dehydroxylation process rises progressively, the peaks corresponding to the hexagonal brucite $\text{Mg}(\text{OH})_2$ become smaller, and the cubic MgO phase starts to appear. After calcination at 400°C, all reflections due to the brucite $\text{Mg}(\text{OH})_2$ disappear, while those corresponding to the MgO phase increase in intensity (Fig. 1(c)-(e)).

Proposed formation mechanism of the prepared materials

Based on SEM and TEM observations, a possible mechanism is proposed in order to explain the formation of the nanostructured $\text{Mg}(\text{OH})_2$. The surfactants are usually used to prepare metal oxide nanoparticles, in which the polar groups directly interact with the particles surface and strongly influence the shape. CTAB is a cationic surfactant which can be adsorbed on the surface of $\text{Mg}(\text{OH})_2$ and can acts as a directing agent by the interaction of positively charged head groups (CTA^+) with hydroxyl groups (O-H) (Fig. 6). The ad-

sorbed CTAB surfactant on the nanocrystal faces which is parallel to the *c* axis could prevent the solute diffusion to the faces. The growth kinetics along the lateral facet is therefore considerably restricted, which mean that the nucleus grow in a one-dimensional (1D) mode and then producing a nanorods shape. During the thermal treatment of $\text{Mg}(\text{OH})_2$, the undecomposed surfactant molecules still retain the shape and the size of $\text{Mg}(\text{OH})_2$ precursors and can act as template morphology to induce the small MgO nanocrystals (Fig. 3(c)). Then, the morphology of $\text{Mg}(\text{OH})_2$ precursor was well preserved in the MgO nanocrystallites during the thermal treatment as indicated in Fig. 3(c).

In order to study the influence of surfactant on the morphology of $\text{Mg}(\text{OH})_2$ products, the synthesis process was conducted under hydrothermal method in the same conditions, without using CTAB as morphology directing agent. Indeed, without CTAB, only magnesium hydroxide nanoplatelets are obtained. Fig. 3(d) depicts the high-resolution TEM image of some individual nanoplatelets. The reason for formation of these nanoplatelets is that the brucite $\text{Mg}(\text{OH})_2$ has a layered structure comprised of sheets as indicated in Fig. 5. The sheets parallel to the *ab* plane are bonded to one-other by weak O-H...O hydrogen bonds. Therefore, the absence of surfactant effect, the nucleuses have the tendency to grow and to aggregate together along the appropriate *ab* plane giving rise to a thin nanoplatelet shape. Ling et al. synthesized the $\text{Mg}(\text{OH})_2$ nanoplatelets using the solvothermal method without using any surfactants or organic templates [20].

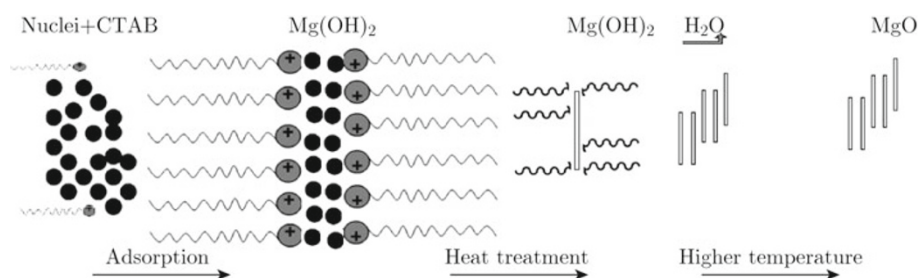


Fig. 6 Schematic illustration of the formation mechanism of MgO nanorods.

Antibacterial activity

The screening of the antimicrobial activity of $\text{Mg}(\text{OH})_2$ nanorods was examined against different microorganisms in the present study. Figure 7 shows zone diameter of inhibition observed for both $\text{Mg}(\text{OH})_2$ nanorods and the control *Ampicillin*. Table 1 summarizes the diameter of the zone of growth inhibition of the studied bacteria strains. The obtained results reveals that the antibacterial activity of the $\text{Mg}(\text{OH})_2$ nanorods against (*Streptococcus B (Streptococcus agalactiae)* and *Bacillus subtilis*) is comparable to that observed for the control sample suggesting

a strong antibacterial activity. While, the antibacterial efficiency of $\text{Mg}(\text{OH})_2$ nanomaterials against the bacterial growth (*Staphylococcus aureus* ATCC 6538, *Enterococcus faecalis* ATCC 29212, *Enterococcus faecium* ATCC 19434, *Bacillus cereus*, and *Staphylococcus faecalis*) is lower than that of the control *Ampicillin* antibiotic suggesting a moderate antibacterial activity against these type bacteria strains. The analysis of these results suggests that the suspension of $\text{Mg}(\text{OH})_2$ nanorods react on the surfaces cell walls that can be disrupted. In fact, the mechanism of this antimicrobial effect may be that proposed by Chunxu and al. [21], which is due to the adsorption of water moisture on

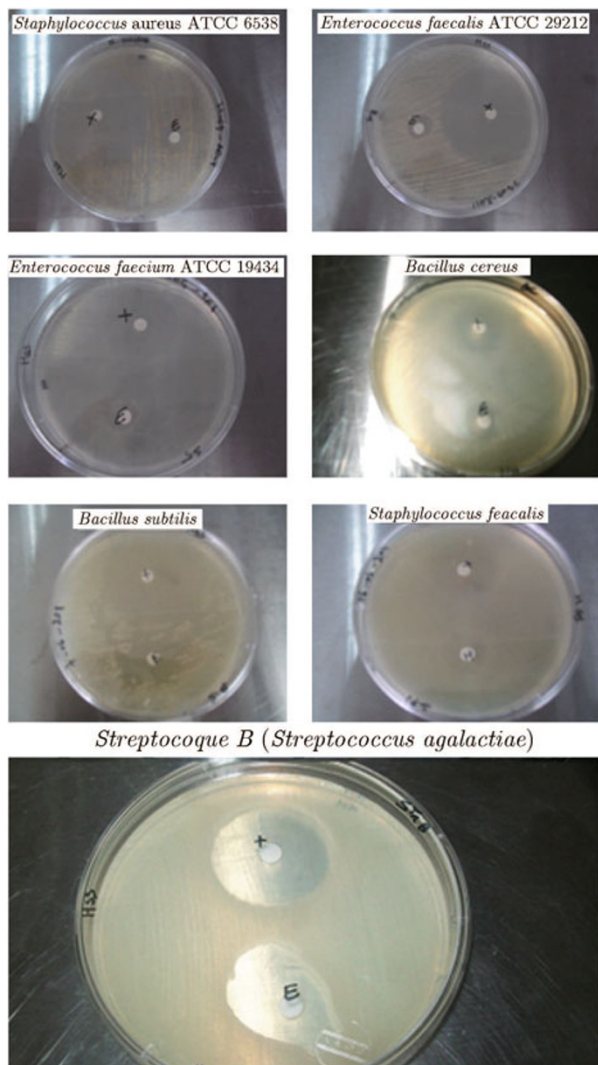


Fig. 7 Diameter zone growth inhibition of $Mg(OH)_2$ nanorods.

Table 1 Antibacterial activity of $Mg(OH)_2$ nanorods.

Strain	Diameter (mm)	
	Ampicillin	$Mg(OH)_2$ suspension
Streptococcus B (<i>Streptococcus agalactiae</i>)	30±2.0	24±1.4
Bacillus subtilis	31±1.5	21±0.7
Bacillus cereus	26±3.2	16±3.5
Staphylococcus aureus (ATCC 6538)	45±3.8	16±1.4
Enterococcus faecium (ATCC 19434)	35±1.5	15±0.7
Staphylococcus faecalis	26±1.5	15±1.4
Enterococcus faecalis (ATCC 29212)	45±3.5	12±1.5

$Mg(OH)_2$ nanomaterials surface, which can form a thin water meniscus around the particles through capillary

condensation. The pH of this thin water layer formed around the nanoparticles may be much higher than the equilibrium medium of the inhibited strains. When the nanoparticles are in contact with the bacteria, the high concentrated OH^- groups in this thin surface water layer could damage the membrane, leading to the perturbation of different cellular processes, and then the leakage of cytoplasm, resulting in the death of the cells.

Conclusion

Pure $Mg(OH)_2$ nanorods have been successfully synthesised from the raw material MgO , using hydrothermal treatment in the presence of surfactant as template agent (CTAB). The as prepared phase shows uniform nanorods shape with a diameter of about 10-40 nm and a length of up to 300 nm. The slow calcination process leads to the MgO product, which has a nanometric character and nanorods shape. The morphology of $Mg(OH)_2$ precursor have been well preserved in the MgO nanocrystallites during the heat treatment. The antimicrobial studies reveal that $Mg(OH)_2$ nanorods constitute an effective antibacterial agent.

References

- [1] Y. Ding, G. Zhang, H. Wu, B. Hai, L. Wang and Y. Qian, Chem. Mater. 13, 435 (2001). <http://dx.doi.org/10.1021/cm000607e>
- [2] Anheuser Busch Inc., US Patent US3839320-A, 1974.
- [3] Mitsubishi Rayon Co. Ltd. (MITR-C). Japan Patent JP52105653-A, 1977.
- [4] Y. Li, M. Sui, Y. Ding, G. Zhang, J. Zhuang and C. Wang, Adv. Mater. 12, 818 (2000). [http://dx.doi.org/10.1002/\(SICI\)1521-4095\(200006\)12:11<818::AID-ADMA818>3.0.CO;2-L](http://dx.doi.org/10.1002/(SICI)1521-4095(200006)12:11<818::AID-ADMA818>3.0.CO;2-L)
- [5] J. C. Yu, A. W. Xu, L. Z. Zhang, R. Q. Song and L. Wu, J. Phys. Chem. B 108, 64 (2004). <http://dx.doi.org/10.1021/jp035340w>
- [6] C. L. Yan, D. F. Xue, L. J. Zou, X. X. Yan and W. Wang, J. Cryst. Growth. 282, 448 (2005). <http://dx.doi.org/10.1016/j.jcrysgro.2005.05.038>
- [7] S. M. Zhang and Zeng H. C., Chem. Mater. 21, 871 (2009). <http://dx.doi.org/10.1021/cm8028593>
- [8] S. A. Davis, M. Breulmann, K. H. Rhodes, B. Zhang and S. Mann, Chem. Mater. 13, 3218 (2001). <http://dx.doi.org/10.1021/cm011068w>
- [9] M. Salerno, J. R. Krenn, A. Hohenau, H. Ditlbacher, G. Schider, A. Leitner, and al., Opt. Commun. 248, 543 (2005). <http://dx.doi.org/10.1016/j.optcom.2004.12.023>
- [10] X. J. Wang, X. L. Qiao, J. G. Chen, H. S. Wang and S. Y. Ding, J. Ceram. (In Chinese) 24, 39 (2003).
- [11] M. Fang, J. H. Chen, X. L. Xu, P. H. Yang and H. F. Hildebrand, Int. J. Anti-microb. Agents, 27, 513 (2006). <http://dx.doi.org/10.1016/j.ijantimicag.2006.01.008>

- [12] C. Dong, D. Song, J. Cairney, O. L. Maddan, G. He and Y. Deng, *Mat. Res. Bul.* 46, 576 (2011). <http://dx.doi.org/10.1016/j.materresbull.2010.12.023>
- [13] H. P. Klug and L. E. Alexander, *X-Ray Diffraction Procedures*, Wiley-Interscience, New York, 1974.
- [14] K. Shinoda, M. Yamakata, T. Nanba, H. Kimura, T. Moriwaki, Y. Kondo, T. Kawamoto, N. Niimi, N. Miyoshi and N. Aikawa, *Phys. Chem. Miner.* 29, 396 (2002). <http://dx.doi.org/10.1007/s00269-002-0243-9>
- [15] H. S. Jung, J. K. Lee, J.Y. Kim and K. S Hong, *J. Colloid Interf. Sci.* 259, 127 (2003). [http://dx.doi.org/10.1016/S0021-9797\(03\)00034-1](http://dx.doi.org/10.1016/S0021-9797(03)00034-1)
- [16] A. C. Chapman, L. E. Thirlwell, *Spectrochim. Acta Cryst.* 20, 937 (1964).
- [17] L. Hao, C. Zhu, X. Mo, W. Jiang, Y. Hu, Y. Zhu and Z. Chen, *Inorg. Chem. Comm.* 6, 229 (2003). [http://dx.doi.org/10.1016/S1387-7003\(02\)00725-6](http://dx.doi.org/10.1016/S1387-7003(02)00725-6)
- [18] P. Ding and B. Qu, *Mat. Lett.* 60, 1233 (2006). <http://dx.doi.org/10.1016/j.matlet.2005.10.111>
- [19] S. Supothina, P. Seeharaj, S. Yoriya and M. Sriyudthsak, *Ceram. Intern.* 33, 931 (2007). <http://dx.doi.org/10.1016/j.ceramint.2006.02.007>
- [20] Z. Ling, M. Zheng, Q. Du, Y. Wang, J. Song, W. Dai, L. Zhang, G. Ji and J. Cao, in press, *Solide State Sciences*. [doi:10.1016/j.solidstatesciences.2010.01.013](https://doi.org/10.1016/j.solidstatesciences.2010.01.013).
- [21] C. Dong, J. Cairney, Q. Sun, O. Lee Maddan, G. He and Y. Deng, *J. Nanopart. Res.* 12, 2101 (2010). <http://dx.doi.org/10.1007/s11051-009-9769-9>